

# MODULATION OF SHORT WAVES BY LONG WAVES

ALLAN M. REECE, JR.\*

*Coastal and Oceanographic Engineering Laboratory, University of Florida, Florida, U.S.A.*

(Received 22 July, 1977)

**Abstract.** The amplitude, wavelength, and frequency of short waves in the presence of waves of a longer scale vary in a manner that is related in phase to the long-wave profile. The purpose of this study is to observe and quantify the change in the variance of short-wave slope that occurs as a result of the change in short-wave position along a coincident long wave, during the active generation of the short-wave field by wind. To this end, measurements of wave-slope time series are made in a laboratory environment where the long-scale waves are generated mechanically and the short scale are generated primarily by air flow. The frequency variation of the short waves, as measured along the long-wave profile, is described by considering the waves to be linearly advected by the longer waves. The peak-to-peak variation along the long-wave profile of the short-wave slope variance for a given frequency band is commonly found to be 100% of its mean value. The magnitude of the excursions become smaller as short-wave frequency increases, and larger as wind speed increases. The maximum value of the short-wave slope variance generally leads the long-wave profile curve by  $45^\circ$  to  $180^\circ$ .

## 1. Introduction

An understanding of how short waves evolve and interact with other waves is essential to the advancement of two principal areas of oceanographic research. Firstly, the field of remote sensing of oceanic parameters is presently undergoing a period of intense development. In many instances short waves are sensed remotely. Of special interest here is the remote sensing of atmospheric and oceanic parameters by airborne and spaceborne radar. Transmitted microwaves interact with water waves of short wavelength through the mechanism of Bragg scattering (Crombie, 1955). If the response of the short waves to the wind and wave conditions were known, the wind and sea state could be inferred from the radar return.

Secondly, short-wave activity can play a major role in the development of an ocean-wave spectrum. Short-wave modulation by long waves is now considered a possible mechanism for transmission of energy to longer waves through a variable-stress mechanism. Longuet-Higgins (1969) demonstrated that a fluctuating tangential stress at the free surface is dynamically equivalent to a normal stress fluctuation lagging the tangential stress by  $90^\circ$ . This results from a change in boundary-layer thickness brought about by the fluctuation in the tangential stress. Wu (1968) found experimentally that, at low wind speeds at least, surface roughness is related to short-wave size and distribution. Many investigators over a long period of time (Keller and Wright, 1975; Cox, 1958; Russell, 1844) have observed that short waves do vary along a long-wave profile. If the short waves were to vary cyclically along a sinusoidal long-wave profile in such a manner that the wind shear reached a maximum near the long-wave crest, a normal stress maximum would

\* Now at Shell Development Company, Houston, Texas.

appear on the rear face of the long-wave crest. The correlation product of this pressure with the local vertical surface velocity would lead to an additional net inflow of energy to the long-wave motion.

The thrust of the present study is toward the investigation of cyclic short-wave energy changes, related in phase to the long wave, which occur during active generation of the short-wave field by wind. To accomplish this objective, experimental measurements of time series of the short-wave slope were made in a laboratory, where the basic long-wave parameters could be controlled as desired and the wind speeds could be accurately reproduced.

## 2. Wave Tank and Instrumentation

Wave-slope measurements were undertaken in the University of Florida wave tank (see Figure 1) to observe the relationship between periodic modification of the short-wave system and long-wave phase. The measurement of slope is advantageous, as it emphasizes the high-frequency portion of the spectrum.

Waves of two scales were created in the wave tank. Waves of 2.0-s period and 10-cm height were generated by a hydraulically powered, mechanical system. Smaller scale waves were generated by an air flow. Wave slopes were measured using a laser-optical system, which senses the results of optical refraction at the air-water interface at a fetch of 7.3 m. Figure 2a illustrates the measurement configuration. The measured angle of laser-beam deflection away from the vertical,  $\phi$ , is related to the local surface slope,  $\theta_i$ , by

$$\theta_i(t) = \tan^{-1} \left[ \frac{\sin \phi(t)}{n - \cos \phi(t)} \right], \quad (1)$$

where  $n$  is the relative index of refraction. Figure 2b schematically depicts the receiver portion of the measurement system. It consists of an aluminum housing containing four essential components: the objective lens, diffusing screen, imaging lens, and photodiode detector. The refracted laser beam passes through the objective lens and is incident on the diffusing screen placed in the rear focal plane.

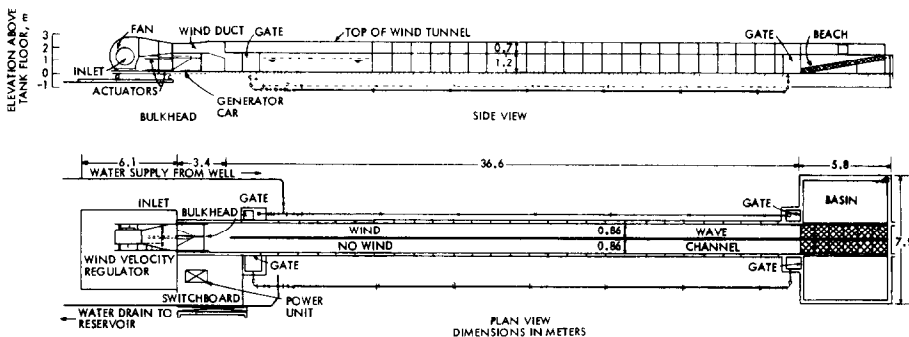


Fig. 1. Plan and side view of wind-wave facility.

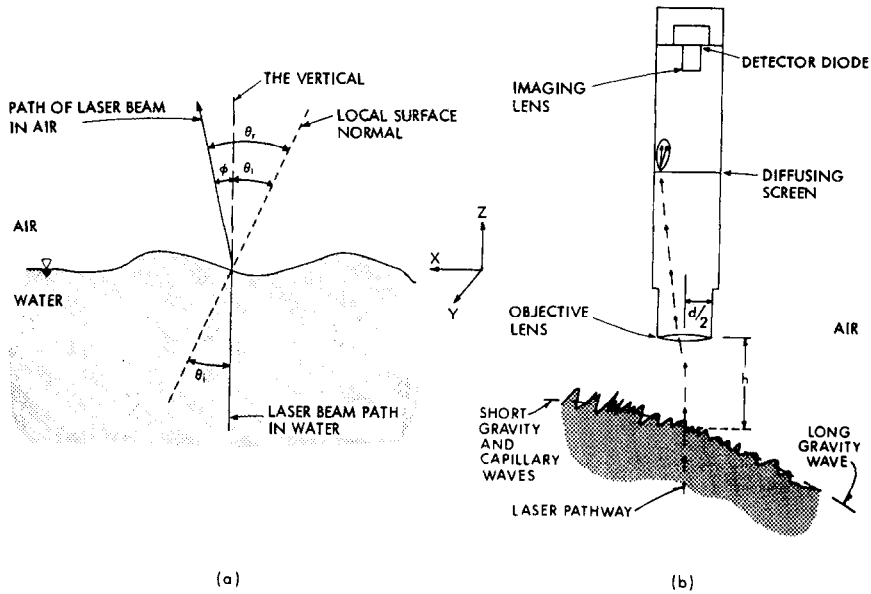


Fig. 2. (a) Schematic diagram of laser beam refraction geometry at air-water interface. (b) Schematic view of the receiver of the optical wave slope measurement system.

The deflection distance of the light beam from the instrument axis is directly proportional to the deflection angle,  $\phi$ , of the light beam. The light scatters from the screen to the imaging lens and is focused on the small 3.56-cm square area of the detector photodiode, to yield electrical signals that are proportional to the deflection distance of the light beam from the axis of the instrument.

### 3. Data Acquisition and Reduction

The signals for long-wave height, upwind-downwind slope component, and sum and difference output of the slope detector were recorded on a Hewlett Packard FM tape recorder model 3960A. The data were then sampled at 400 Hz without prefiltering, and recorded on digital magnetic tape. The digitized data were used to obtain mean short-wave spectra and the modulation of short-wave spectra over the profile of a long mechanically-generated wave. A central aim of the analysis was to produce stable estimates of short-wave slope spectra at selected regions along the long-wave profile. This was done by averaging ensembles of spectra, each of which was calculated from a length of record corresponding to a specific phase location along the long-wave profile.

The experimental conditions under which data were taken are shown in Table I. For each of the nine test conditions, sufficient data were recorded to obtain 133 long-wave cycles for use in the analysis. The analysis, designed to obtain spectral estimates along the long-wave profile, proceeded as follows. The positive-going zero crossing of long-wave height was located for each long-wave cycle. Starting at

TABLE I  
Experimental test conditions

Experiment designation	Reference wind ( $\text{m s}^{-1}$ )	Local wind at 7.3-m fetch ( $\text{m s}^{-1}$ )	$U_*$ at 7.3-m fetch ( $\text{m s}^{-1}$ )	Wave Period (s)	Wave Height (cm)
1	3.8	2.7	0.099	2.0	10.0
2	4.4	3.4	0.110	2.0	10.0
3	4.9	3.5	0.127	2.0	10.0
4	5.6	4.0	0.145	2.0	10.0
5	5.9	4.2	0.153	2.0	10.0
6	7.2	5.1	0.187	2.0	10.0
7	8.3	5.7	0.223	2.0	10.0
8	9.2	6.5	0.239	2.0	10.0
9	10.1	7.2	0.262	2.0	10.0

Date: September 18, 1975; Time: 12:00 p.m.

each positive-going zero crossing, the total wave-slope time series was divided into eight overlapping segments, as shown in Figure 3. A cosine bell function was applied to the first and last 10% of the data points in each segment, to prepare the segment for conversion to the frequency domain. A Fast Fourier Transform (FFT) algorithm provided the conversion. For tests when the wind speed was less than  $5.9 \text{ m s}^{-1}$ , it was felt that since spectral resolution was low, it would be prudent to remove the large, low-frequency component of slope introduced by the long-wave profile. So the trend appearing in each segment, due to long-wave slope, was removed by fitting a polynomial to the segment and subtracting it from each data point. At higher wind speeds, the wind-wave slopes were large enough to obscure the long-wave trend. The eight spectra that result from this analysis are each assumed to be representative of the wind-waves at the phase location central to the corresponding time series segment.

Eight spectra were calculated for each of the 133 long-wave cycles. Each of the 256 point spectra had a frequency resolution of 1.56 Hz. Eight ensembles were formed, each containing spectra from a common phase location along the long-wave profile. The average of the 133 spectra contained in each ensemble provided

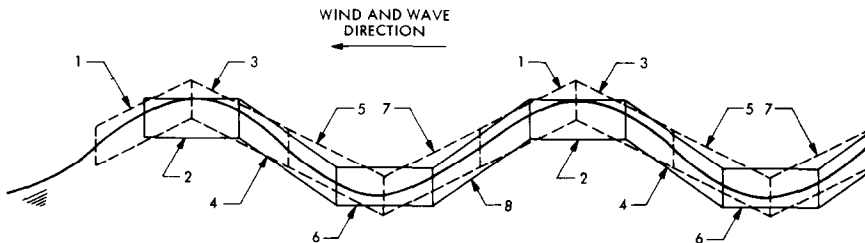


Fig. 3. Wave-record segmenting scheme used to produce short-wave-slope time series at specific long-wave-phase locations for subsequent spectral analysis.

the final estimate for the short-wave slope spectrum to be associated with a given phase location along the long-wave profile. The stability of the spectral estimates obtained in this manner is specified in terms of equivalent degrees of freedom of the approximating chi-square distribution (Welch, 1967). The number of equivalent degrees of freedom were found to be 266. The associated 80% confidence limits, expressed as ratios of the limits to the average values, are 0.88 and 1.13 (Blackman and Tukey, 1958).

#### 4. Experimental Results

##### TIME SERIES DATA

The time series displayed in Figure 4 illustrate the effects that the long-wave motion has on the short-wave field at a friction velocity,  $U_*$ , of  $18.7 \text{ cm s}^{-1}$ . A reference air flow velocity was measured at the center of the channel cross-section at a point 8-m upstream of the measurement location. For this particular case, the reference wind speed was measured to be  $7.2 \text{ m s}^{-1}$ . The interdependence of the long- and short-wave fields results in two distinguishable effects on the short-wave field. Firstly, if one considers the envelope containing the slope maxima and minima, it is clearly seen that the envelope width is not constant and is, in fact, related to the long-wave phase. Secondly, the frequency range of the short-wave field varies along the long-wave profile. Both wind-wave frequencies and slope envelope widths reach maximum values in the vicinity of the front face of the long waves. We designate these effects frequency and amplitude modulations.

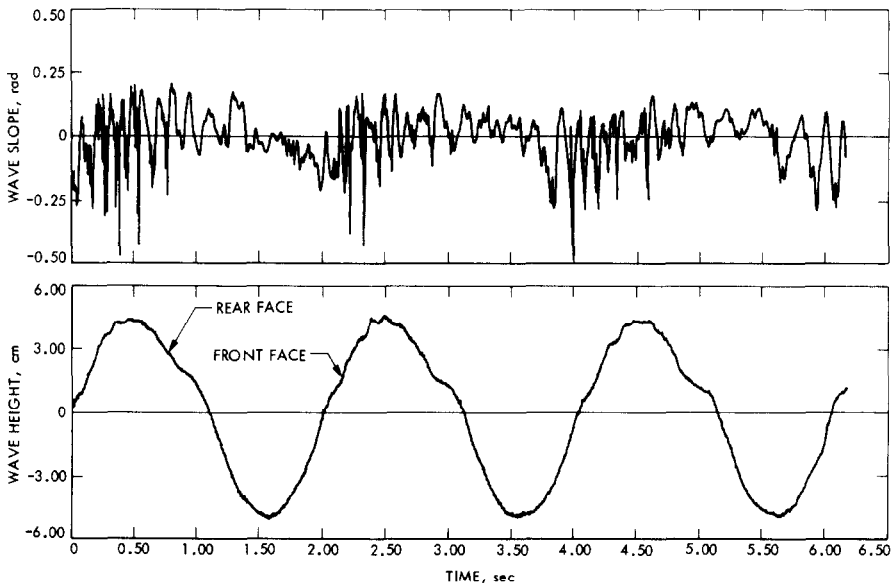


Fig. 4. Wave slope, measured along the axis of the mean wind, and wave height as functions of time for a fetch of 7.3 m and a reference wind speed of  $7.2 \text{ m s}^{-1}$ .

### MEAN WAVE-SLOPE SPECTRA

Mean wave-slope spectra are calculated using an FFT algorithm on the entire wave-slope time series, and are used to establish a reference value for the short-wave steady-state energy. The spectral transformation provides a frequency resolution of about 0.1 Hz and a stability of 93 equivalent degrees of freedom. The associated 80% confidence limits, expressed as ratios of the limits to the average values, are 0.81 and 1.19 (Blackman and Tukey, 1958).

Figure 5 illustrates the effects of changing wind speed on the slope spectra. The error bars on the dotted curves mark the 80% confidence limits, and apply to the other two curves as well. All of the spectra show an increase in the slope variance with increasing wind speed. It is seen from the series of spectra that the first and second harmonics of the long wave, appearing at 0.977 and 1.465 Hz, respectively, are altered at the higher wind speeds, while the fundamental, which appears at 0.488 Hz, remains unchanged. The intensity level of the first harmonic increases slightly at the highest wind speeds, while the second harmonic decreases with increasing wind; so that above  $10.1 \text{ m s}^{-1}$  wind speed, it is reduced to the level of the wind-driven portion of the spectrum.

The data in time-series form indicate an abrupt increase in the slope amplitudes for a reference wind speed around  $5.0 \text{ m s}^{-1}$ . A frequency-by-frequency comparison of the spectra calculated for  $4.9$  and  $5.6 \text{ m s}^{-1}$  shows that from the lower to the higher speed, substantial increases in slope variance occur in the frequency regions from 2.0 to 10.0 Hz and 20.0 to 60.0 Hz. The 2.0 to 10.0 Hz region shows the most striking increase.

The highest value of the wind-driven portion of the spectrum is reached in the frequency band at 3.22 Hz. In the region from 2.0 to 10.0 Hz, the spectra tend to develop a plateau, where the spectral values do not vary greatly with frequency. In the middle range of wind speeds, a second plateau begins to form in the 20.0 to 70.0 Hz region. As wind speed increases further, the region between the two fills in, as a result of rising slope amplitudes, and eliminates the second plateau.

### SPECTRAL MODULATIONS

In order to use the available spectral information to quantify short-wave modulation, it is necessary to discriminate between the effects of amplitude and frequency modulation. The overall change in the shape of the short-wave slope spectra, as a function of phase along the long-wave profile, is illustrated in Figure 6 for a wind speed of  $4.9 \text{ m s}^{-1}$ . The error bars in the figure apply for each curve and represent the 80% confidence limits. Note that the curve representing the spectrum calculated at the long-wave crest is similar in shape to, but located considerably to the right of, the curve representing the spectrum calculated for the trough.

If the shift in frequency of each spectral estimate were quantified, it would be possible to identify the remainder of the spectral variation related to the long wave as an amplitude modulation of the intensity level within a selected frequency band.

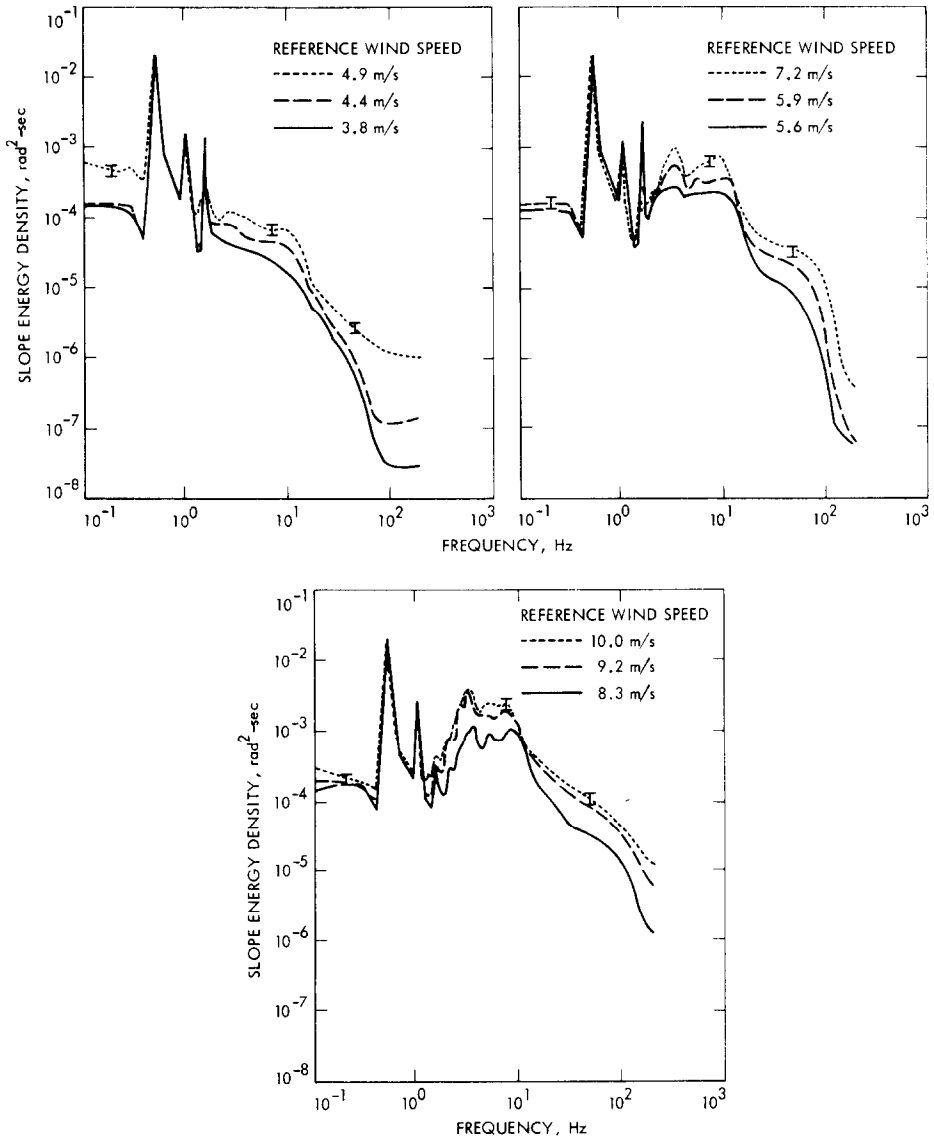


Fig. 5. Averaged wave-slope spectra for the complete wave system. Wind speed ranged from 3.8 to 10.1  $\text{ms}^{-1}$ .

The frequency modulation may be approximated by the calculation of local frequency based on the changing short-wave phase speed,  $C_s(x)$ , corresponding to the local wavenumber,  $k_s(x)$ . For this formulation, the long-wave orbital velocity,  $U_l(x)$ , is specified at the surface, to first order, by

$$U_l(x) = a_l \sigma_l \sin(k_l x), \tag{2}$$

where  $a_l$ ,  $\sigma_l$ , and  $k_l$  are the long-wave amplitude, frequency, and wavenumber,

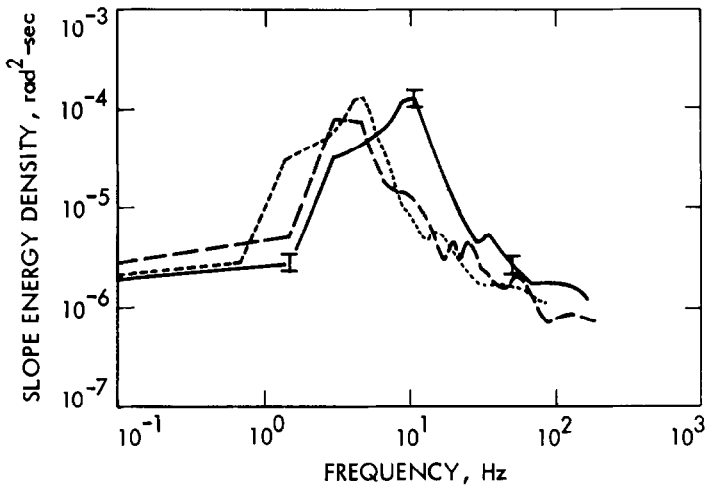


Fig. 6. Phase-averaged spectra of short-wave slope from crest and trough regions of the long wave for a wind speed of  $4.9 \text{ m s}^{-1}$ , long-wave height of  $10.0 \text{ cm}$  and a period of  $2.0 \text{ s}$ . — short-wave spectrum at long-wave crest; - - - short-wave spectrum at long-wave trough; ..... short-wave spectrum at long-wave crest, frequency corrected for advection.

respectively.  $x$  represents the distance from the zero crossing on the rear of a crest of a steady long-wave profile. The wind-drift velocity,  $U_d$ , is assumed to be constant at the surface. The velocity of propagation of a short wave,  $C_s(x)$ , to first order in wave slope, may be written

$$C_s(x) = C_0 + U_l(x) + U_d, \quad (3)$$

where  $C_0$  is the short-wave phase speed calculated from linear theory. Retaining terms of order  $(a, k_l)^0$ , the corresponding frequency modulation may be written

$$\omega_s(x) = \omega_0(k_0) + k_0\{U_l(x) + U_d\}, \quad (4)$$

where  $k_0$  is the unmodified short-wave wavenumber and  $\omega_0$  is the frequency from the linear wave-dispersion relation relating to  $k_0$ . The dotted curve of Figure 6 represents the spectrum calculated at the long-wave crests shifted in frequency, by the amount indicated by Equation (4), to the long-wave troughs, using a wind-drift velocity of 3% of the reference wind speed (Shemdin, 1972). Sinitsyn's (1973) good results with the linear expression for frequency above indicate that it is reasonable to use it here to approximate the frequency shift.

#### AMPLITUDE MODULATION OF THE SPECTRUM

Figure 7a illustrates, for the test at  $4.9 \text{ m s}^{-1}$  wind speed, the total spectral variation that occurs along the long-wave profile for the selected frequencies,  $\omega_0/2\pi = 9.38, 12.50, \text{ and } 15.63 \text{ Hz}$ . To construct Figure 7a, the values of spectral density corresponding to the frequencies shown in the figure key are plotted at each of the eight phase locations along the long-wave profile at which they were calculated.

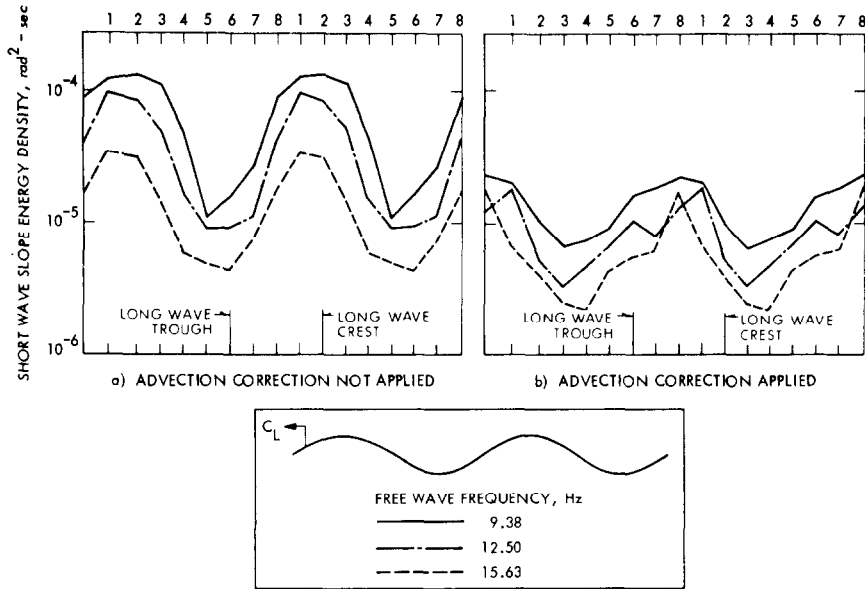


Fig. 7. Short-wave-slope energy density modulated by long waves. Wind speed =  $4.9 \text{ m s}^{-1}$ , long-wave height =  $10.0 \text{ cm}$ , long-wave period =  $2.0 \text{ s}$ . (a) Without correction for advection, (b) With correction for advection.

The spectral values are obtained from the spectra computed at each phase location without regard to the fact that the frequency of an individual wave, if it existed, would be modified according to position along the long-wave profile. The figure shows that the excursions of the spectral values are large relative to the mean value of each selected frequency band, and that the peaks occur in the region of the long-wave crests. Figure 7b displays the results from the same test as Figure 7a, but the frequencies are corrected for advection in accord with Equation (4). The wave frequency,  $\omega_s(x)$ , related to  $\omega_0$  by Equation (4), is then used to obtain spectral values from each of the eight spectral calculations along the long-wave profile. The curves of Figure 7b are identified by their relation to  $\omega_0$ , but are actually associated with  $\omega_s(x)$  and take into account the effect of advection by the underlying flow. The spectral variations indicated in Figure 7b represent the amplitude modulation of the short-wave slope spectrum induced by the long wave in the frequency band identified by the frequencies in the figure key.

The amplitude modulation values at different unmodified frequencies,  $\omega_0$ , are shown in Figure 8 for wind speeds of  $4.4$  and  $10.1 \text{ m s}^{-1}$ . The corresponding phase shifts with respect to the long wave are shown in the top part of the figure. For both wind speeds, the amplitude modulation decreases with increasing frequency. The phase shifts vary between  $45^\circ$  and  $180^\circ$  downwind of the crest.

The wind dependence of the amplitude modulation values is depicted in Figure 9 for the two frequencies  $\omega_0/2\pi = 9.38$  and  $20.0 \text{ Hz}$ . The spectral modulation amplitude increases with increasing wind speed.

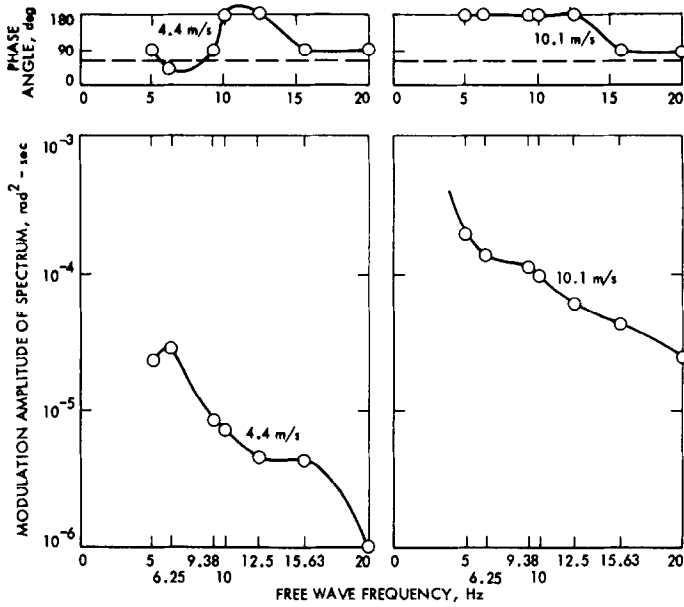


Fig. 8. Magnitude and phase of short-wave-slope energy spectrum modulation at the indicated frequencies and at wind speeds of 4.4 and 10.1 m s<sup>-1</sup>. Phase angles are measured forward of a long-wave crest.

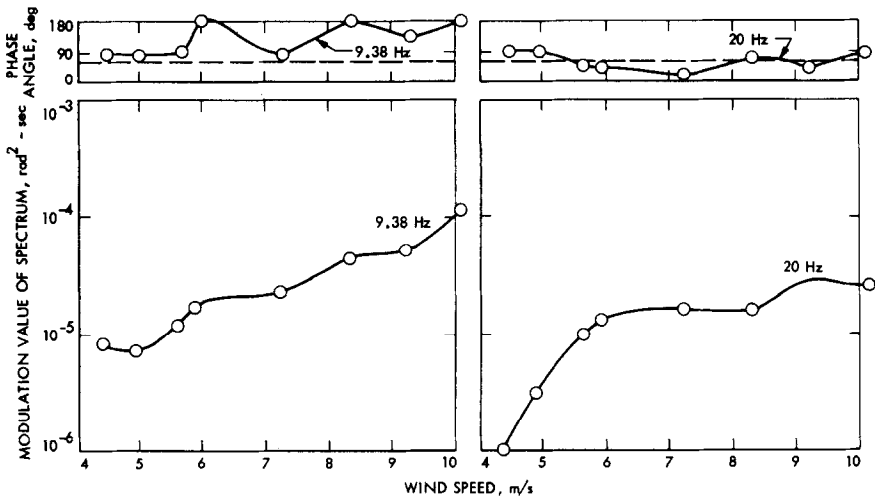


Fig. 9. Wind-speed dependence of short-wave-slope energy spectrum modulation magnitude and phase at frequencies of 9.38 and 20.0 Hz. Phase angles are measured forward of a long wave crest.

One may do a rough comparison of these results with those of Keller and Wright (1975). The radar that they used in their experiment responded to changes in short water waves with an unmodified frequency of 10.4 Hz. Their data indicate that for a  $U_*$  of 20 cm s<sup>-1</sup>, the ratio of slope spectral excursion from its mean value to its

mean value is approximately 0.305. In the present experiment at a  $U_*$  of  $18.7 \text{ cm s}^{-1}$ , the 10.0-Hz wave varied in the ratio of 0.338. At a  $U_*$  of  $10 \text{ cm s}^{-1}$ , the Keller and Wright wave-slope energy varied in the ratio of 0.333. In the present experiment at a  $U_*$  of  $11.0 \text{ cm s}^{-1}$ , the 10.0-Hz wave varied in the ratio of 0.726. The results show order-of-magnitude agreement; in addition there is agreement that the ratio increases with decreasing friction velocity.

## 5. Conclusions

The results contained in this paper apply to wind-generated waves with frequencies from 5.0 to 20.0 Hz superimposed on a mechanical wave with wave height of 10.0 cm and wave period of 2.0 s, while the wind speed ranged from 4.4 to  $10.1 \text{ m s}^{-1}$ . Within these experimental bounds, the short-wave slope variances were found to exhibit cyclic variations that are related to the phase of the long wave. The variations result from two combined effects: the short-wave frequency is varied by the long-wave orbital velocity; and the energy of the short waves is modulated by the actions of aerodynamic and hydrodynamic couplings that operate on the short waves in a manner that is related to long-wave phase.

The frequency modulation of the short waves, although complicated by uncertainties in the local wind drift and the local long-wave orbital velocity, is described by considering the waves to be linearly advected by the longer waves. The mean frequency shift is that due to the steady underlying wind-driven current. The mean shift was found to vary from 40 to 126% of the unadverted frequency, increasing as the unadverted frequency increased and as the wind speed increased. The frequency modulation was predicted to increase with an increase in  $\omega_0$ , the unadverted frequency, and to equal 58% of that frequency for the long wave considered.

The amplitude of the wave-slope energy modulation is considered after compensating for the frequency modulation based on surface drift and orbital velocities. The peak-to-peak variation of the energy in a frequency band of the wave-slope spectrum due to the amplitude modulation effect is commonly 100% of the mean value of the energy found as the average of all values for that frequency band along the wave profile. The magnitude of the excursions become smaller as short-wave frequency increases, and larger as wind speed increases. The experimentally determined phase relationship between the long-wave profile and the slope energy variation of a short-wave frequency band falls between  $45^\circ$  and  $180^\circ$  with the intensity modulation leading. There is a slight trend toward larger phase angles with increasing wind speed.

## Acknowledgment

This paper is based on a Ph.D. dissertation which the author wrote at the University of Florida. He is indebted to Dr O. H. Shemdin for selecting the problem and

directing the research effort. Dr Charles S. Palm is responsible for the design and construction of the wave-slope optical measurement system.

The study was supported by NOAA-Space Oceanography Program under Grant NG-29-72 and by JPL under Contract 954030.

### References

- Blackman, R. B. and Tukey, J. W.: 1958, *The Measurement of Power Spectra*, Dover Publications, New York.
- Cox, C. S.: 1958, 'Measurements of Slopes of High Frequency Wind Waves', *J. Marine Res.* **16**, 199-225.
- Crombie, D. D.: 1955, 'Doppler Spectra of Sea Echo at  $13.56 \text{ mc s}^{-1}$ ', *Nature* **175**, 681-682.
- Keller, W. C. and Wright, J. W.: 1975, 'Microwave Scattering and the Straining of Wind-Generated Waves', *Radio Sci.* **10**, 139-147.
- Longuet-Higgins, M. S.: 1969, 'A Non-Linear Mechanism for the Generation of Sea Waves', *Proc. Roy. Soc.* **A311**, 371-389.
- Russell, J. S.: 1844, 'Report of the Committee on Waves', *Proc. British Assoc. Advanced Sci.*, Seventh Meeting, York, 1844, 311-390.
- Shemdin, O. H.: 1972, 'Wind-Generated Current and Phase Speed of Wind Waves', *J. Phys. Oceanog.* **2**, 411-419.
- Sinitsyn, Y. A., Leykin, I. A., and Rozenberg, A. D.: 1973, 'The Space-Time Characteristics of Ripple in the Presence of Long Waves', *Izvestiya Atmos. Ocean. Phys.* **9**, 511-519.
- Stewart, R. W.: 1961, 'The Wave Drag of Wind over Water', *J. Fluid Mech.* **10**, 189-194.
- Welch, P. D.: 1967, 'The Use of Fast Fourier Transforms for the Estimation of Power Spectra: A Method Based on Time Averaging over Short, Modified Periodograms', *IEEE Trans. on Audio and Electro Acoustics*, **AU-15**, No. 2, 70-73.
- Wu, F.: 1968, 'Laboratory Study of Wind-Wave Interactions', *J. Fluid Mech.* **34**, 91-111.